Assessing heat exposure to extreme temperatures in urban areas using the Local Climate Zones classification

Joan Gilabert[1,2,3], Anna Deluca[4], Dirk Lauwaet[5], Joan Ballester[4], Jordi Corbera[2], Maria Carmen Llasat[1]

[1]GAMA Team Department of Applied Physics - University of Barcelona,

[2] Institute Cartographic and Geological of Catalonia (ICGC),

[3]URBAG research team, Sostenipra SGR 1412 ICTA-UAB,

[4]Climate and Health Program - Barcelona Institute for Global Health, [4]Flemish Institute for Technological Research (VITO)

Correspondence to: Joan Gilabert (jgilabert@meteo.ub.edu)

Abstract. Trends of extreme temperature episodes in cities are increasing (in frequency, magnitude and duration) due to regional climate change in interaction with the urban effects. Urban morphologies and thermal properties of the materials used to build them are factors that influence the spatial and temporal climate variability and becomes one of the main reasons for the climatic singularity of cities. This paper presents a proposal to evaluate the urban and peri-urban effect on extreme temperatures exposure in Barcelona (Spain), using the Local Climate Zone (LCZ) framework as a base statement, that allows the comparison with other cities of the world characterized using this criterion. LCZs were introduced as input of the high resolution UrbClim model (100 m spatial resolution) to create the daily temperatures (median and maximum) series for summer (JJA) during the period 1987 to 2016, pixel by pixel, in order to create a cartography of extremes. Using the relationship between mortality due to high temperatures and the temperature distribution, the heat exposure of each LCZ was obtained. Methodological results of the paper show the improvement obtained when LCZs were mapped through a combination of two techniques (from Land Cover/Land Use maps and from WUDAPT method), as well as proposes a methodology to obtain the exposure to high temperatures of different LCZs on urban and peri-urban areas. In the case of Barcelona, the distribution of temperatures for the 90th percentile (about 3-4ºC compared to average conditions) leads to an increase in the relative risk of mortality of 80%.

1. Introduction

Alterations to the natural environment associated with urban activity mean that climate variability in urban landscapes is more complex than in peri-urban and rural areas. Urban landscapes are home to more than half the world's population and projections show that two-thirds of the world's population will live in cities by 2050 (UN, 2015). Urban areas are certainly more exposed and vulnerable to the negative effects of climate change due to their non-sustainable relationship with surrounding areas and environments. The Urban Climate Change Research Network's Second Assessment Report on Climate Change in Cities (ARC 3.2) (Rosenzweig et al., 2018), places the average annual temperature increase ratio per decade between 0.12 and 0.45ºC in the period from 1961 to 2010. And it is estimated that the temperature will rise between 1.3 and 3ºC towards 2050 and 1.7 to 4.9ºC in 2080.

Urban landscapes are particularly sensitive to rising temperatures at all timescales (Pachauri RK et al., 2014). Heat waves (HW) are one of the deadliest weather events and their frequency, intensity and duration are expected to increase in the future due to climate change (Li and Bou-Zeid, 2013; De Jarnett and Pittman, 2017; Sheridan and Dixon, 2016) and the urban heat island (UHI) effect. Consequently, the related health impacts are of emerging environmental health concern (Wolf and McGregor, 2013). In Europe, the growing urbanisation along with the impacts of the increasing of extreme temperature causes increased heat-related mortality (Smid et al., 2019; Ingole et al., 2020).

There are many factors that influence the spatial and temporal climate variability in urban areas, such as different urban morphologies and the thermal properties of the materials used to build them (Geletič et al., 2016; Li et al., 2016). One of the main topics usually studied to characterise the urban climate are the extreme temperatures in cities due to UHI effect, which was first discussed back in the 1940s (Balchin and Pye, 1947). Historically, a considerable body of research has been published on the phenomenon (i.e, Oke, 1982; Lo et al., 1997; Arnfield, 2003; Voogt and Oke, 2003; Chen et al., 2006; Mirzaei and Haghighat, 2010; Giannaros et al., 2014; Lehoczky et al., 2017; Sobrino and Irakulis, 2020). However, certain methodological inconsistencies have been revealed when comparing different urban climate studies. One of the main reasons is the lack of standardisation to compare the properties that affect specific urban thermal behaviour

65   (Stewart, 2011). Moving forward from this premise, a new methodology based on the

66   Local Climate Zone (LCZ) classification has emerged (Stewart and Oke, 2012). LCZ

67   establishes a system of standardisation for urban and rural areas and their thermal

68   responses. LCZ proposes a classification with a total of 17 measurable categories based

69   on a combination of geometric, thermal, radiative and metabolic parameters that

70   characterise urban and peri-urban areas (Fig. S1). By using this classification, it is

71   possible to study the effects of urban climate in more spatial and temporal detail (Bechtel

72   et al., 2015). The combination of built environment (Benzie et al., 2011; Inostroza et al.,

73   2016) is well encompassed by the LCZ approach, and, along with socio-demographic

74   factors (Nayak et al., 2018), this allows us to develop a geospatial distribution of heat

75   exposure (Dickson et al., 2012; Drobinski et al., 2014). Along the same line of research,

76   the international project called World Urban Database and Access Portal Tools

77   (WUDAPT) has created a portal with guidelines based on earth observation data, with the

78   aim of building a worldwide database of cities, using the LCZ classification. This

79   standardisation will allow comparisons between cities, while providing better data for

80   meteorological and climate models (Brousse et al., 2016; Ching et al., 2018). Currently,

81   the available, validated layer for Barcelona on the WUDAPT portal is the one made in

82   our studio to fill in the Metropolitan Area of Barcelona (AMB), as explained in more

83   detail in section 3.1.

84   Although the LCZ was originally designed to describe the radiative characteristics of the

85   different land covers and land uses, it can also be applied to estimate the level of heat

86   exposure to adverse climate conditions. There are a wide range of definitions for the term

87   'vulnerability' (UNISDR, 2009; Cutter, 1996; Llasat et al., 2009), which depend on

88   different physical and social factors (Cutter et al., 2000; Tromeur et al., 2012; Nakamura

89   and Llasat, 2016). In this framework heat vulnerability is understood as a combination of

90   heat exposure (based on high temperatures) and sensitivity (Wolf and McGregor, 2013;

91   Bao et al., 2015; Inostroza et al. 2016), where the last is related with the population

92   characteristics and coping capacities. Although there are some publications that study risk

93   on an urban scale for extreme heat events (Xu et al., 2012; Weber et al., 2015; Krstic et

94   al., 2017; Eum et al., 2018), few have been studied from an LCZ perspective. This paper

95   therefore aims to assess heat exposure using the LCZ classification in a coastal

96   Mediterranean metropolitan region. Barcelona constitutes a good example of a

97   Mediterranean coastal megacity (port cities with a population greater than 1 million in

98 2005) (Hanson et al., 2011) that can be severely affected by climate change impacts. In
99 effect, annual mean temperature increase in the Mediterranean Basin is higher than the
100 world average (1.5ºC above 1880-1899 in 2018) and could be above 2.2ºC in 2040
101 without additional mitigation (Lionello et al., 2014; Cramer et al., 2018; MedECC, 2019).
102 Direct impacts on health produced by the frequency and intensity increase of heat waves
103 and tropical nights will be amplified by the urban heat island effect, particularly important
104 in Barcelona (Baccini et al, 2011; Martin-Vide and Moreno, 2020). Associated to this
105 temperature increase, by 2050, for the lower sea-level rise scenarios and current
106 adaptation measures, cities in the Mediterranean will account for half of the 20 global
107 cities with the highest increase in average annual damages (Hallegate et al., 2013).

108 The paper is divided into two main chapters. The first deals with the study area, data and
109 proposed methodology. The second, is focused on applying the methodology to the city
110 of Barcelona and showing the respective results. The paper ends with a section on
111 discussion and conclusions.

112 This study is a starting point for new research lines with three objectives in mind: a)
113 making changes to urban land cover and observing the changes in heat exposure to high
114 temperatures without having to resort to climate modelling; b) downscaling the
115 temperature outputs of urban models to resolutions under 100m using the LCZ maps; c)
116 applying this methodology to climate change scenarios.

117 **2. Data and Methods**

118 **2.1. Study area**

119 The Metropolitan Area of Barcelona (AMB) and its surroundings have been selected to
120 apply the LCZ classification. AMB involves the city of Barcelona and 35 adjoining
121 municipal areas (Fig. 1). The AMB is situated in the northwest of the Mediterranean basin
122 and covers an area of 636 km^2 with a population of around 3,2 llion. The city of
123 Barcelona (~1,6 million) is in its centre, between the Llobregat River (South), the Besòs
124 River (North), the Catalan Coastal Range (West) and the Mediterranean Sea (East) (Fig.
125 1b).

126 The Barcelona municipality has been selected to analyse the effect of high temperatures
127 and apply the proposed methodology approach on a neighbourhood scale. Barcelona is

128   divided into 10 districts, which are subdivided into 73 neighbourhoods. It covers an area

129   of 101 km^2 and has a population density of over 15,000 inh./km^2, which is higher than

130   New York City, Tokyo or New Delhi. In terms of climate, Barcelona and its surroundings

131   are characterised by hot summers (25ºC-27ºC average temperature), and the thermal

132   stress of high temperatures is accentuated by the proximity of the sea, which results in a

133   humid atmosphere. Total precipitation in Barcelona is around 600 mm per year. Autumn

134   is the wettest season and has a highly irregular distribution of precipitation, in many cases

135   causing episodes of urban flooding (Gilabert and Llasat, 2017; Cortès et al., 2018).

136

137   2.2 Methodology design

138   In order to carry out this study, we followed the workflow shown below:

139   1. LCZ Mapping: A GIS methodology based on Land Cover and Land Use (LCLU)
140   maps has been applied to the entire AMB to improve the precision of the
141   international WUDAPT method. The WUDAPT method has been also applied to
142   all the area showed in Figure 1b, both inside and outside AMB, that will be used
143   as input of the climate model.
144   2. Climate characterisation of the median and extreme temperature distribution in
145   Barcelona from the outputs of UrbClim model.
146   3. Defining the heat exposure thresholds based on the epidemiological temperature-
147   mortality model proposed by Achebak et al. (2018).
148   4. Developing a methodology for the thermal characterisation of the LCZs and its
149   assessment.

150   Each one of these steps will be explained in detail in the following sections in order to

151   simplify the understanding of this methodology in which each part is based in the results

152   of the previous one. The own methodology followed constitutes a result of this work.

153   2.3. LCZ mapping

154   2.3.1 Data from official thematic cartography, satellite images and weather stations

155 In order to create the LCZ cartography data showed in Table 1 have been used. The LCZs

156 were represented following two methods, as explained in section 3. The Land Cover Land

157 Use method was based on using all the layers presented in Table 1, except for the Landsat

158 8 image, which was only used with the WUDAPT methodology and the orthophoto to

159 make the training areas.

160 **2.3.2 Land Cover and Land Use method and WUDAPT method**

161 There are several proposals for mapping LCZs, whether from a bottom up or top down

162 approach (Brousse et al., 2016; Lelovics et al., 2014; Wang et al., 2017; Mitraka et al.,

163 2015). Each LCZ is defined by 10 variables (geometric, radiative and metabolic), which

164 were tested and standardised by Stewart and Oke (2012) and are applied in this study.

165 Our study features a LCZ map that combines two different mapping techniques (Fig. 2).

166 For the administrative region of the AMB (with a more extensive and detailed source of

167 data), a methodology based on LCLU data was used that departs from the reclassification

168 of the land use key for the existing high-resolution maps. The LCLU data were combined

169 with LIDAR data, which allowed us to define the height of the buildings. There are other

170 techniques that use similar methodologies to show LCZs, like those by Geletič and

171 Lehnert (2016) or Skarbit et al. (2017). For the area outside the AMB, the international

172 WUDAPT methodology was used, based on satellite earth observation data (Bechtel et

173 al, 2015). This study improved accuracy through a population map and high resolution

174 orthophotos provided by the Cartographic and Geological Institute of Catalonia (ICGC).

175 Both methodologies are summarized below.

176 The LCLU method is based on different Land Cover and Land Use maps (see Table 1),

177 such as the Land Cover Map of Catalonia (LCLU-Cat), which uses an extensive

178 classification of up to 241 categories (CREAF, 2010), and the Urban Atlas (UA) (EEA,

179 2010). The first thematic map was used to define the Land Cover Types and density of

180 vegetation. The UA distinguishes 20 categories of urban areas and discerns between urban

181 fabric type and density, which is why it is very useful for the first 10 categories of LCZ.

182 Each LCLU category corresponds to one of the descriptions of the different

183 morphological parameters that define the LCZ. The Building Heights is another layer of

184 the map, and was made with a LIDAR sensor, which was also used to discern between

185 the different Urban Climate Zones.

186 Figure 3 shows the difference between the total coverage of each LCZ when obtained

187 from the LCLU and from WUDAPT maps in AMB (Fig. 2). In the WUDAPT approach,

188 52.8% of the surface area of the AMB consists of urban areas (LCZ 1-10 and E), while

189 in the high-resolution map (LCLU approach), the same type of coverage occupies just

190 37.3% due to the different resolution of both methodologies. In both methods, we can

191 see that the natural forest category (LCZ-A) is the most common, accounting for 24.1%

192 and 18.4% of the land respectively. This is due to the fact that the AMB includes

193 Collserola Natural Park in the Coastal Mountain Range. The next most common class is

194 LCZ-C, which corresponds to scrubland and bush. Dealing with land classified as urban,

195 the most common types include industrial estates (LCZ-8), areas with dense buildings

196 less than 25 m tall (LCZ-2) and category LCZ-6, which consists of open arrangements of

197 mid-rise buildings. The WUDAPT map suffers from a lack of characterisation of urban

198 areas, which is not the case for the LCLU map.

199 The resulting LCZ map is a high resolution thematic/vector map/base map (Figure 2b),

200 in which each polygon that makes up the urban fabric is attributed to an LCZ category

201 (Gilabert et al., 2016). Finally, it was rasterised at a resolution of 100 m, applying an all

202 shape filter, so that it could be used as an input for the UrbClim model. The method we

203 followed is shown in the workflow diagram (Figure 4). There are similar examples in the

204 literature, such as the LCZ map for the Ïle-de-France (www.institutparisregion.fr), or the

205 LCZ-LCLU Map of Vienna (Hammerberg et al., 2018).

206 The WUDAPT method (Bechetel et al., 2015) allows us to create a 100 m x 100 m raster

207 map based on earth observation data from remote sensing. The representative regions of

208 interest are chosen for proposed LCZ categories from earth observation satellite data, with

209 the use of very high resolution aerial orthophotos as a ground truth. The LCZ map, made

210 by the first author of this paper, using the WUDAPT proposal, is officially presented on

211 the project portal and is available for download (www.wudapt.org). This method has been

212 applied to an extended area as is showed at Figure 5.

213 A multi-resolution grid shape file (62.5 m, 125 m and 250 m) containing information on

214 the population as registered in 2016 (IDESCAT, 2018) was used to correct the peri-urban

215 areas of AMB where rural activities cannot see well identified. The orthophoto was used

216 to check and correct any categories and the limits between them.

217 Figure 5 shows the resulting map combining the LCLU method (in raster format) for the
218 administrative region of the AMB, and WUDAPT method for the rest of the study area
219 with a final resolution of 100m.

2.4 Weather stations

221 Table 2 shows the weather stations within the municipality of Barcelona that have been
222 used to evaluate and compare the characterization of the LCZ with the daily average
223 temperature outputs of the UrbClim model. LCZ and height information are also attached.

2.5 UrbClim model simulation

225 UrbClim is an Urban Boundary-Layer Climate Model specifically designed to simulate
226 temperature at a very high spatial resolution (here at 100 m; De Ridder et al., 2015). The
227 model consists of a land surface scheme with simplified urban physics coupled to a 3D
228 atmospheric boundary layer. UrbClim is faster than high-resolution mesoscale climate
229 models by at least two orders of magnitude (García-Díez et al., 2016), making the very
230 long runs that are necessary for climate change related studies possible. UrbClim has been
231 recently validated in several European cities, including Barcelona (García-Díez et al.,
232 2016). Currently, within the framework of the Pan-European Urban Climate Service
233 (PUCS) project (H2020, 2017-2010), the urban climate of Barcelona has been modelled
234 until 2100, keeping in mind different Representative Concentration Pathways (RCPs) to
235 observe the consequences of climate change on an urban scale. Barcelona was chosen,
236 among other European cities, and VITO and ISGlobal were the organisations responsible
237 for modelling this city.

238 UrbClim model uses a land-surface and a soil-vegetation-atmosphere transfer scheme that
239 is designed to deal with urban surfaces. Each surface grid cell in the model is made up of
240 portions of vegetation, bare soil and urban surface cover, which are all represented using
241 LCZ mapping. A set of transfer equations, together with appropriate parameter values for
242 albedo, emissivity, aerodynamic and thermal roughness length are used to simulate the
243 heat transfer in each surface grid cell. The large-scale atmospheric conditions are used as
244 lateral and upper boundary conditions. The 3D boundary layer model represents a
245 simplified atmosphere by using the continuity equations for horizontal momentum,
246 potential temperature, specific humidity and mass.

247 The simulations for the 1987-2016 period were used for this period. The UrbClim
248 simulations cover a large domain containing 401x401 horizontal grid points at 100 m
249 resolution (40x40 km approximately), and 19 vertical levels within the lower 3 km of the
250 troposphere. It covers the entire geographical area of the Metropolitan Area of Barcelona,
251 including the neighbouring highly populated cities. The driving model data are updated
252 every 3 hours using ERA-Interim reanalysis (Dee et al., 2011), which runs at a spatial
253 resolution of T255 (approximately 70-80 km). The UrbClim model directly downscales
254 the ERA-Interim reanalysis data to 100 m resolution. The climate distribution of the daily
255 mean temperature (Tmean), maximum temperature and dew point temperatures were
256 calculated for all the summer months (JJA). The dew point temperature (Tdew) was used
257 as a starting point to calculate the HUMIDEX Eq. (1) that describes the perceived thermal
258 feeling of a person, by combining the effect of heat and humidity (Masterton and
259 Richardson, 1979). Barcelona has quite a high relative humidity during the summer
260 months, which means that the HUMIDEX increases considerably.

261 $HUMIDEX = T_{mean} + 0.5555 \left[6.11 e^{5417.7530 \left(\frac{1}{273.16} + \frac{1}{273.15 + T_{dew}} \right)} - 10 \right]$ Eq. (1)

262 **2.6 Quantifying heat exposure by temperature**

263 The next step consists of reclassifying the maps of the proposed distributions for the daily
264 mean temperature, keeping in mind the impact that they can have on the health. This was
265 carried out using the results provided in the study by Achebak et al. (2018), in which a
266 distributed lag nonlinear model was used to model the short-term delayed relation
267 between daily summer temperature and mortality data from cardio-respiratory diseases in
268 Barcelona (and 46 other cities), over a similar period of time modelled (Fig. 6). This
269 makes it possible to objectively establish the thresholds for health relative risks (RR),
270 based on temperature. For instance, a RR value of 1.20 means that the relative risk of
271 mortality is 20% higher at a given level of temperature exposure compared to a baseline
272 optimum temperature (e.g. temperature of minimum mortality, when RR=1). Relative
273 risks are statistically significant when the lower bound of the CI is greater than 1.

274 We are assuming that the curve is applicable to all districts of the city (Achebak et al.,
275 2018). Table 3 has been built for RR intervals of 0.2 (20%) following the Figure 6. Each
276 RR interval has been associated to a Heat Exposure Index (HEI) that includes temperature

277 interval based on the curve of Achebak et al. (2018). Barcelona deals with HEI value of
278 1 for temperatures between 18 and 20ºC up to a HEI value of 7, for temperatures above
279 31.1ºC that would mean a very high relative risk of mortality associated with high
280 temperatures.

3. Results

3.1 UrbClim temperature outputs and HEI maps

283 In order to analyse the impact of the different LCZ in the distribution of high temperatures
284 in summer the maps of maximum and daily mean temperature corresponding to
285 percentiles P50, P75, P90, P95 and P99 have been built (Fig. 7). Barcelona has a high
286 relative humidity due to proximity to the sea that increases the warm perception, and, for
287 this reason, the cartography of the average daily HUMIDEX value has also been
288 represented.

289 As we can see in figure 7, there is a very similar spatial distribution pattern. The lowest
290 temperatures are in the most remote area of the coast and they are mainly associated with
291 categories LCZ A and LCZ 9 (mainly covering areas of woodland or very low-density
292 buildings). A cooling effect can also be noted in the most important parks in the city, as
293 well as on the seafront, because of the sea breeze (the UrbClim model underestimates the
294 sea breeze effect in Barcelona, García-Diez et al., 2016). The highest temperatures can be
295 found in the centre of the city, with a tendency to increase in a north-easterly direction.

296 We saw that P99 of HUMIDEX reached 39ºC. In Barcelona, without taking humidity into
297 account, the average temperature in the city can reach above 30ºC. Even so, normal
298 temperatures during the summer are around 27ºC. In Mediterranean cities, relative
299 humidity is important since it is usually high, a fact that affects temperature (Diffenbaugh
300 et al., 2007). In this sense, we observe that the HUMIDEX can register temperatures of
301 the order of 5ºC higher than the sensible temperature. Anyway, this study has focused on
302 sensible temperature because the curve that defines the HEI has been made for sensible
303 temperature. In any case, we must bear in mind that the temperature or heat stress may be
304 higher due to the greater HUMIDEX.

305 Figure 8 shows maps of HEI distribution reclassified the UrbClim output of daily mean
306 temperature according to the proposed thresholds showed in section 2.6. This

307 reclassification turns the extreme temperature maps or hazard maps into heat exposure
308 maps. It can be seen that the HEI is lower in areas with higher altitude and in inter-urban
309 parks (as the Montjuïc Park located in SE of the map), although when P90 is surpassed,
310 the HEI value goes over level 5 for most of the urban fabric. Note that the P50 shows an
311 increase in the relative risk of mortality of 40%.

312 **3.2 Thermal characterisation of the LCZs**

313 In this section we aim to match up each LCZ with a determined thermal behaviour to
314 create a methodology that will allow us to estimate the heat exposure to high temperatures
315 from this data.

316 First, we analysed the thermal response of the LCZ (LCZ-T) to the high temperature
317 situations obtained in the climate analysis (Fig. 7). Second, we analysed the probability
318 density curves for each LCZ, so that we could calculate the anisotropy levels of the LCZs.
319 Using this foundation, we built curves for the LCZs and a defined scenario for the
320 percentiles considering the HEI, which allowed us to create a model that was applicable
321 not only to Barcelona but also to other regions with similar behaviour. Transposing the
322 model on LCZ maps allows us to map heat exposure distributions for Barcelona.

323 Figure 9 shows that LCZ 8, 1, E and 2 (from highest to lowest), have usually the highest
324 temperatures. These LCZ in general terms correspond to the categories with high
325 admittance and high permeability (Stewart and Oke, 2012). In contrast, the lowest
326 temperatures correspond to LCZ 9, A, C and G, which are wooded areas and parks on the
327 outskirts of the city. On the other hand, crops and bare land (LCZ C and F) show very
328 variable behaviour, as during the day they tend to be surfaces that store and retain heat,
329 while during the night their behaviour registers temperatures under the average of the
330 sample. These surfaces are characterised by a large temperature range given the marked
331 contrast between day and night.

332 Table 4 shows that the more extreme the percentile the larger the standard deviation, as
333 expected. Besides this, the more marked deviations correspond to LCZ C and F, which
334 correspond to wooded or bare areas and which show less thermal inertia. On the other
335 hand, category C is very highly influenced (in the case of Barcelona) by orientation, as
336 there are zones located in shaded parts of valleys while other zones are in the sunny ones,

337 which has a direct impact on the deviation. In the case of category C, we observed that it

338 corresponds to a land use that is not very representative in spatial terms.

3.3 Mapping the heat exposure with LCZs

340 Figure 10 shows the average behaviour of the LCZs for different temperature percentiles

341 (P50, P75, P90, P95, P99). The values corresponding to range between the 25th and 75th

342 percentiles of each LCZ for each probability scenario have been adjusted to a logarithmic

343 curve that can be very useful to build heat exposure maps for high temperatures based on

344 the thermal properties of the LCZ. Knowing the temperature distribution for each

345 category and scenario allows doing the simulation of the impact on temperature

346 distribution of potential modifications to the urban morphology.

347 As explained in the methodology, seven ranges of temperature have been defined

348 according to different relative risk thresholds (Table 3) established by the curve proposed

349 in the study by Achebak et al. (2018) (Fig. 6). By characterising the LCZ from the model

350 represented in Figure 11, the maps of the heat exposure index (HEI) associated to high

351 temperatures for different probabilistic scenarios have been built. The scenario

352 corresponding to the P75 of the temperature would imply a ratio of relative risk of

353 mortality increase of 60%, and, 80% in a scenario according to the P90.

3.4 Assessment and comparation of the LCZ-T relationship

355 The results of the LCZ-T relationship as well as the results of the Urban Climate model

356 (UC) have been compared with the distribution of temperature obtained from series of

357 over 10 years for five weather stations (Table 2) located in different LCZ in the

358 municipality of Barcelona. RMSE and the differences between the output of both

359 (UrbClim model and LCZ-T relationship) and observations have been obtained in order

360 to compare the results (Tables 5 and 6). We want to highlight that the UrbClim has been

361 already validated in Barcelona by García-Díez et al. (2016) as outlined in section 2.6.

362 Table 5 shows that differences in absolute value are lower than 1.2ºC. In all the cases they

363 are equal or below 0.5 ºC for the percentile of 50, and also for the percentile of 75 with

364 the exception of the Raval station, that is placed in the oldest part of the city. It should

365 also be kept in mind that a standalone observation is not the same as an aerial 100 x 100

366 m observation, and this fact is particularly important when the weather station is
367 surrounded by buildings.

368 The HEI maps drawn up using the LCZs were compared with the map based on
369 temperature distributed created by UrbClim (Table 6). Coincidences between pixels for
370 both models are above 80% for percentiles P50, P75 and P90, and more than 60% in all
371 cases.

372

373 **4. Discussion and conclusions**

374 Along this paper a methodology to characterize the distribution of daily mean temperature
375 for the different LCZs in different scenarios has been proposed. This characterization has
376 been done for the summer months and climate percentiles have been obtained for the
377 period 1987-2016 and applied at 100 m resolution to the city of Barcelona. Although
378 other authors have already worked with the relationship between thermal behaviour and
379 LCZ category (Stewart et al., 2014; Skarbit and Gal., 2015; Geletič et al., 2016; Verdonck
380 et al., 2018) they have usually applied Land Surface Temperature satellite images, for the
381 summer months and a short time period. Other characterizations of LCZ using weather
382 stations can also be found in Alexander and Mills (2014) and Kotharjar and Bagade
383 (2018). In this case, these authors have worked with climate series from observational
384 data. The advantage of the methodology proposed here, in which the LCZ distribution
385 has been compared with the outputs of a high-resolution climate model (UrbClim) is that
386 the relationship has been established from long climate series and for the entire selected
387 region. Currently, there are quite a few studies characterizing LCZs using urban model
388 outputs (Aminipouri et al., 2019; Beck et al., 2018; Geletič et al., 2018; Kwok et al., 2019;
389 Unger et al., 2018), but there are few that do it with climatic outings that span so many
390 years.

391 The results of this methodology applied to the Metropolitan Area of Barcelona have
392 showed a major difference between the thermal response in summer for the different LCZ
393 that this obtained from some satellite images. In terms of land use, LCZ A and C, that
394 belong to the most prevalent categories, show the lowest temperatures, consistent with
395 the majority of studies carried out (e.g. Geletič et al., 2016). In our case, category C

396 shows a wider interquartile range than the other types. This is because this category is
397 found in different altitudes along the Catalan Coastal Range and in areas with different
398 orientations. Regarding category B, attributed to the majority of interurban parks, it
399 maintains temperatures below those of the most typical urban zones.

400 The highest daily mean summer temperatures in Barcelona are concentrated in LCZ 2, E,
401 1, 8 F and 10, with LCZs 2, 1 and E being the most representative of the urban planning
402 in the city centre. With regard to LCZ 8 and 10, these are zones that tend to record high
403 temperatures due to the nature of the activities and materials on the land cover (in the
404 most cases, metal structures). The urban LCZ with the lowest temperatures is 9, which is
405 almost non-existent in Barcelona and is located mainly in zones in the Catalan Coastal
406 Range with a significant altitudinal slope. Another urban LCZ with low relative
407 temperatures commonly found in the city is 6, which is mainly located in the
408 neighbourhoods furthest away from the coast and closer to the mountain. These
409 neighbourhoods have a higher percentage of urban green cover, less dense buildings and
410 one of the highest per capita GDPs in the city.

411 The paper has also introduced the Heat Exposure Index (HEI), that evaluates the increase
412 of the risk of mortality ratio as a consequence of heat exposure in basis to the model
413 proposed by Achebak et al. (2018) which connects relative risk of mortality caused by
414 cardio-respiratory failure with the effects of high temperatures. This index, associated to
415 each LCZ once the temperature has been associated to it, allows mapping the HEI. The
416 comparison between the HEI maps elaborated directly from the temperature outputs
417 produced by the UrbClim model and those produced from LCZ cartography is well-suited
418 to simulate them for scenarios corresponding to percentiles of temperature between 50%
419 and 90%, and, in the case in which there is no coincidence between the HEI value in the
420 pixel, it is more usual underestimation than overestimation. In the case of Barcelona, the
421 distribution of temperatures for the P90 (about 3-4ºC compared to average conditions)
422 leads to an increase in the relative risk of mortality of 80%, and 40% in the case of P50.

423 This paper also provides comparison of two methodologies to cartography the Local
424 Climate Zones (LCZ). The study area has been mapped using two techniques, the LCLU
425 based on land use maps and the WUDAPT. The LCLU has been applied to the
426 Metropolitan Area of Barcelona and the WUDAPT to the entire region (inside and
427 outside) the AMB. The WUDAPT map suffers from a lack of characterisation of different

428 types of urban areas, which is not the case for the LCLU. Then, when the required data is
429 available it is better to apply the LCLU methodology than the WUDAPT one. In this
430 study, the curve of Achebak et al. (2018) was taken into account, as representative of the
431 whole of Barcelona city. In the future, it would be good to have a similar curve for
432 different districts of the city. However, in future work it would be interesting to represent
433 a sensitivity map taking into account coping capacities based on GDP, social structure of
434 the neighbourhood, etcetera. This would include vulnerability.

435 In conclusion, the LCZ-T relation based on the characterisation of the average
436 temperature for each LCZ corresponding to different percentile distribution, allows us to
437 consider adaptive methods, proposing changes to more sustainable urban planning, for
438 example the use of green or white cover. The advantage of the proposed methodology is
439 that it allows to obtain a heat exposure distribution for summer temperatures without
440 having to resort climate models, by applying the model of temperature distribution
441 associated to each LCZ. It can be also useful to do different experiments modifying land
442 uses and land coverages over the cartography, and, consequently, the LCZ distribution
443 and their associated HEI. Another possibility is being able to separate the heat exposure
444 levels on an LCZ map with higher spatial resolutions to those used in weather models and
445 climate models.

Acknowledgements

447 This publication was supported by the Industrial Doctorate Programme (ref. 2015-DI-
448 038) between the University of Barcelona and the Cartographic and Geological Institute
449 of Catalonia, the Water Research Institute (IdRA) at the University of Barcelona, M-
450 CostAdapt (CTM2017-83655-C2-2-R) research projects (MINECO/AEI/FEDER, UE)
451 and ERC Consolidator Grant awarded to Gara Villalba (818002-URBAG). The authors
452 would like to thank the European Environment Agency (EEA), Centre for Ecological
453 Research and Forestry Applications (CREAF) and Metropolitan Area of Barcelona for
454 the land use maps available. We would also like to thank the State Meteorological Agency
455 (AEMET) and the Meteorological Service of Catalonia (SMC) for the weather station
456 data. Finally, we want to thank Hicham for giving us the RR model.

457 JB gratefully acknowledges funding from the European Union's Horizon 2020 research
458 and innovation programme under grant agreements No 865564 (European Research

459   Council Consolidator Grant EARLY-ADAPT), 727852 (project Blue-Action) and
460   730004 (project PUCS), and from the Ministry of Science and Innovation (MCIU) under
461   grant agreements No RYC2018-025446-I (programme Ramón y Cajal) and EUR2019-
462   103822 (project EURO-ADAPT).

463   **Author contributions**

464   JG conceived the study, designed and carried out the data analysis and wrote the paper.
465   MCL, JC and JB have participated in defining the analysis and methodology, contributed
466   to interpreting the results, and to writing the paper. DL and AdL have run the UrbClim
467   model and prepare the output data.

468   **Competing interests**

469   The authors declare that they have no conflict of interest.

470   **References**

471   Achebak, H., Devolder, D., and Ballester, J.: Heat-related mortality trends under recent
472   climate warming in Spain: A 36-year observational study. PLoS med. 15(7): e1002617,
473   2018.

474   Alexander, P., and Mills, G.: Local climate classification and Dublin's urban heat
475   island. Atmosphere. 5(4): 755-774, 2014.

476   Aminipouri, M., Knudby, A. J., Krayenhoff, E. S., Zickfeld, K. and Middel, A.:
477   Modelling the impact of increased street tree cover on mean radiant temperature across
478   Vancouver's local climate zones. Urban Forestry & Urban Greening, 39, 9–17, 2019.

479   Arnfield, A. J.: Two decades of urban climate research: a review of turbulence, exchanges
480   of energy and water, and the urban heat island. Int. J. Climatol. 23(1): 1-26, 2003.

481   Baccini, M., Kosatsky, T., Analitis, A., Anderson, H.R., D'Ovidio, M., Menne, B.,
482   Michelozzi, P., Biggeri, A.: Impact of heat on mortality in 15 European cities: attributable
483   deaths under different weather scenarios. J Epidemiol Commun H, 65, 64-70, 2011.

484   Balchin, W. G. V., and Pye, N.: A micro-climatological investigation of bath and the
485   surrounding district. Q. J. Royal Meteorol. Soc. 73(317-318): 297-323, 1947.

486   Bao, J., Li, X. and Yu, C.: The construction and validation of the heat vulnerability index,
487   a review. Int. J. Environ. Res. Public Health. 12(7): 7220-7234, 2015.

488   Beck, C., Straub, A., Breitner, S., Cyrys, J., Philipp, A., Rathmann, J., Schneider, A.,
489   Wolf, K. and Jacobeit, J.: Air temperature characteristics of local climate zones in the
490   Augsburg urban area (Bavaria, southern Germany) under varying synoptic conditions.
491   Urban Climate, 25, 152–166, 2018.

492   Bechtel, B., Alexander, P. J., Böhner, J., Ching, J., Conrad, O., Feddema, J., Mills, G.,
493   See, L., and Stewart I.: Mapping local climate zones for a worldwide database of the form
494   and function of cities. ISPRS Int. J. Geo-Inf. 4(1): 199-219, 2015.

495   Benzie, M., Harvey, A., Burningham, K., Hodgson, N., and Siddiqi, A.: Vulnerability to
496   heatwaves and drought: Case studies of adaptation to climate change in South-west
497   England. Joseph Rountree Foundations, 2011.

498   Brousse, O., Martilli, A., Foley, M., Mills, G., and Bechtel B.: WUDAPT, an efficient
499   land use producing data tool for mesoscale models? Integration of urban LCZ in WRF
500   over Madrid. Urban Clim. 17: 116-134, 2016.

501   Chen X. L., Zhao H. M., Li P. X., and Yin Z. Y.: Remote sensing image-based analysis
502   of the relationship between urban heat island and land use/cover changes. Remote Sens.
503   Environ. 104(2): 133-146, 2006.

504   Ching, J., Mills, G., Bechtel, B., See, L., Feddema, J., Wang, X., Ren, C., Brousse, O.,
505   Martilli, A., Neophytou, M., Mouzoudires, P., Stewart, I., Hanna, A., Ng, E., Foley, M.,
506   Alexander, P., Aliaga, D., Niyogi, D., Shreevastava, A., Bhalachandran, S., Masson, V.,
507   Hidalgo, J., Fung, J., de Fatima Andrad, M., Baklanov, A., Wei Dai, D., Milcinski, G.,
508   Demuzere, M., Brunsell, N., Pesaresi, M., Miao, S., Mu, Q., Chen, F., and Theeuwes, N.:
509   World urban data base and access portal tools (WUDAPT), an urban weather, climate and
510   environmental modelling infrastructure for the Anthropocene. Bull. Am. Meteorol. Soc.
511   99(9): 1907-1924, 2018.

512 Cortès, M., Llasat, M. C., Gilabert, J., Llasat-Botija, M., Turco, M., Marcos, R., Martin
513 Vide, J. P., and Falcón L.: Towards a better understanding of the evolution of the flood
514 risk in Mediterranean urban areas: the case of Barcelona. Nat. Hazards. 93(1): 39-60,
515 2018.

516 Cutter, S. L.: Vulnerability to environmental hazards. Prog. Hum. Geogr. 20(4): 529-539,
517 1996.

518 Cutter, S.L., Mitchell, J. T., and Scott, M. S.: Revealing the vulnerability of people and
519 places: a case study of Georgetown County, South Carolina. Ann. Am. Assoc.
520 Geogr. 90(4): 713-737, 2000.

521 Cramer, W., Guiot, J., Fader, M., Garrabou, J., Gattuso, J. P., Iglesias, A., Lange, M. A.,
522 Lionello, P., Llasat, M. C., Paz, S., Peñuelas, J., Snoussi, M., Toreti, A., Tsimplis, M. N.,
523 and Xoplaki, E.: Climate change and interconnected risks to sustainable development in
524 the Mediterranean. Nat. Clim. Change 8:972-980, doi: 10.1038/s41558-018-0299-2,
525 2018.

526 Dee, D. P., Uppala, S. M., Simmons, A. J., Berrisford, P., Poli, P., Kobayashi, S., Andrae,
527 U., Balmaseda, M. A., Balsamo, G., Bauer, P., Bechtold, P., Beljaars, A. C. M., van de
528 Berg, L., Bidlot, J., Bormann, N., Delsol, C., Dragani, R., Fuentes, M., Geer, A. J., Healy
529 S. B., Hersbach, H., Hólm, E. V., Isaksen, L., Kallberg, P., Kölher, M., Matricardi, M.,
530 McNally, A. P., Morcrette, J. J., Park, B. K., Peubey, C., de Rosnay, P., Tavolato, C.,
531 Thépaut, J. N. and Vitart, F.: The ERA-Interim reanalysis: Configuration and
532 performance of the data assimilation system. Q. J. Roy. Meteor. Soc. 137(656): 553-597,
533 2011.

534 DeJarnett, N., and Pittman, M.: Protecting the Health and Wellbeing of Communities in
535 a Changing Climate. Proceedings of a Workshop – in Brief. The National Academies
536 Press. 10.17226/24797, 8p, 2017.

537 De Ridder, K., Lauwaet, D., and Maiheu, B.: UrbClim–A fast urban boundary layer
538 climate model. Urban Clim. 12: 21-48, 2015.

539 Dickson, E., Baker, J. L., and Hoornweg, D.: Urban risk assessments: understanding
540 disaster and climate risk in cities. The World Bank Publications, 2012.

541   Diffenbaugh, N. S., Pal, J. S., Giorgi, F., and Gao, X.: Heat stress intensification in the
542   Mediterranean climate change hotspot. Geophysical Research Letters, 34(11), 2007.

543   Drobinski, P., Ducrocq, V., Alpert, P., Anagnostou, E., Béranger, K., Borga, M., Braud,
544   I., Chanzy, A., Davolio, S., Delrieu, G., Estournel, C., Filali Boubrahmi, N., Font, J.,
545   Grubisic, V., Gualdi, S., Homar, V., Ivancan-Picek, B., Kottmeier, C., Kotroni, V.,
546   Lagouvardos, K., Lionello, P., Llasat, M. C., Ludwig, W., Lutoff, C., Mariotti, A.,
547   Richard, E., Romero, R., Rotunno, R., Roussot, O., Ruin, I., Somot, S., Taupier-Letage,
548   I., Tintore, J., Uijlenhoet, R. and Wernli, H.: HyMeX, a 10-year multidisciplinary
549   program on the Mediterranean water cycle, B. Am. Meteorol. Soc. 95(7): 1063-1082,
550   2014.

551   Eum, J. H., Kim, K., Jung, E. H., and Rho, P.: Evaluation and Utilization of Thermal
552   Environment Associated with Policy: A Case Study of Daegu Metropolitan City in South
553   Korea. Sustainability. 10(4): 1179, 2018.

554   García Díez, M., Lauwaet, D., Hooyberghs, H., Ballester, J., De Ridder, K., and Rodó,
555   X.: Advantages of using a fast urban boundary layer model as compared to a full
556   mesoscale model to simulate the urban heat island of Barcelona. Geosci. Model Dev.
557   9(12): 4439-4450, 2016.

558   Geletič, J., Lehnert, M., Dobrovolný, P.: Land Surface Temperature Differences within
559   Local Climate Zones, Based on Two Central European Cities. Remote Sens. 8(10): 788,
560   2016.

561   Geletič, J., Lehnert, M.: GIS-based delineation of local climate zones: The case of
562   medium-sized Central European cities. Morav. Geogr. Rep. 24(3): 2-12, 2016.

563   Geletič, J., Lehnert, M., Savic, S., and Miloševic, D.: Modelled spatiotemporal variability
564   of outdoor thermal comfort in local climate zones of the city of Brno, Czech Republic.
565   Science of the Total Environment, 624, 385–395, 2018.

566   Giannaros, T. M., Melas, D., Daglis, I. A., and Keramitsoglou, I.: Development of an
567   operational modeling system for urban heat islands: an application to Athens, Greece.
568   Nat. Hazards Earth Syst. Sci., 14(2), 347, 2014.

569 Gilabert, J., Tardà, A., Llasat, M. C., and Corbera, J.: Assessment of Local Climate Zones
570 over Metropolitan Area of Barcelona and added value of Urban Atlas, Corine Land Cover
571 and Copernicus Layers under INSPIRE Specifications. INSPIRE Conference, Barcelona,
572 2016.

573 Gilabert, J., and Llasat, M. C.: Circulation Weather Types associated with extreme flood
574 events in Northwestern Mediterranean. Int. J. Climatol. 38(4): 1864-1876, 2017.

575 Hallegatte, S., Green, C., Nicholls, R. J. and Corfee-Morlot, J.: Future flood losses in
576 major coastal cities. Nat. Clim. Change 3, 802–806, 2013.

577 Hammerberg, K., Brousse, O., Martilli, A., and Mahdavi A.: Implications of employing
578 detailed urban canopy parameters for mesoscale climate modelling: a comparison
579 between WUDAPT and GIS databases over Vienna, Austria. Int. J. of Climatol. 38: 1241-
580 1257, 2018.

581 Hanson, S., Nicholls, R., Ranger, N., Hallegatte, S., Cofree-Morlot, J., Herweijer, C.,
582 Chateau, J.: A global ranking of port cities with high exposure to climate extremes.
583 Climatic Change, 104(1), 89-111, 2011.

584 Ingole, V., Marí-Dell'Olmo, M., Deluca, A., Quijal, M., Borrell, C., Rodríguez-Sanz, M.,
585 Achebak, H., Lauwet, D., Gilabert, J., Murage, P., Hajat, S., Basagaña, X., and Ballester,
586 J.: Spatial Variability of Heat-Related Mortality in Barcelona from 1992–2015: A Case
587 Crossover Study Design. Int. J. Environ. Res. Public Health.17(7): 2553, 2020.

588 Inostroza, L., Palme, M., and de la Barrera, F.: A heat vulnerability index: spatial patterns
589 of exposure, sensitivity and adaptive capacity for Santiago de Chile. PloS one. 11(9):
590 e0162464, 2016.

591 Kotharkar, R., Bagade, A.: Local Climate Zone classification for Indian cities: A case
592 study of Nagpur. Urban clim. 24: 369-392, 2018.

593 Krstic, N., Yuchi, W., Ho, H. C., Walker, B. B., Knudby, A. J., and Henderson, S. B.:
594 The Heat Exposure Integrated Deprivation Index (HEIDI): A data-driven approach to
595 quantifying neighborhood risk during extreme hot weather. Environ. Int. 109: 42-52,
596 2017.

597   Kwok, Y. T., Schoetter, R., Lau, K. K. L., Hidalgo, J., Ren, C., Pigeon, G., and Masson,
598   V.: How well does the local climate zone scheme discern the thermal environment of
599   Toulouse (France)? An analysis using numerical simulation data. International Journal of
600   Climatology, 39(14), 5292-5315, 2019.

601   Lehoczky, A., Sobrino, J. A., Skoković, D., and Aguilar, E.:The Urban Heat Island Effect
602   in the City of Valencia: A Case Study for Hot Summer Days. *Urban Science*, *1*(1), 9,
603   2017.

604   Lelovics, E., Unger, J., and Gál, T.: Design of an urban monitoring network based on
605   Local Climate Zone mapping and temperature pattern modelling. Clim. Res. 60: 51-62.
606   Li D, Bou-Zeid E. (2013) Synergistic interactions between urban heat islands and heat
607   waves: the impact in cities is larger than the sum of its parts. J. Appl. Meteorol.
608   Clim. 52(9): 2051-2064, 2014.

609   Li, X., Li, W., Middel, A., Harlan, S. L., Brazel, A. J, and Turner, B. L.: Remote sensing
610   of the surface urban heat island and land architecture in Phoenix, Arizona: Combined
611   effects of land composition and configuration and cadastral- demographic- economic
612   factors. Remote Sens. Environ. 174: 233-243, 2016.

613   Lionello, P., Abrantes, F., Gacic, M., Planton, S., Trigo, R., and Ulbrich, U.: The climate
614   of the Mediterranean region: research progress and climate change impacts. Reg Environ
615   Change 14, 1679–1684., 2014.

616   Llasat, M. C., Llasat-Botija, M., López, L.: A press database on natural risks and its
617   application in the study of floods in Northeastern Spain. Nat. Hazard. Earth Sys. 9(6):
618   2049-2061, 2009.

619   Lo C. P., Quattrochi, D. A., and Luvall, J. C.: Application of high-resolution thermal
620   infrared remote sensing and GIS to assess the urban heat island effect. Int. J. Remote
621   Sens. 18(2): 287-304, 1997.

622   Martin-Vide, J., and Moreno-Garcia, M. C.: Probability values for the intensity of
623   Barcelona's urban heat island (Spain). Atmos. Res., 104877, 2020.

624 Masterton, J. M., and Richardson, F. A.: Humidex: a method of quantifying human
625 discomfort due to excessive heat and humidity. Environment Canada. Atmospheric
626 Environment, 1979.

627 MedECC.: Risks associated to climate and environmental changes in the Mediterranean
628 region. A preliminary assessment by the MedECC Network. Science-policy interface –
629 2019. 36 pp, 2019.

630 Mirzaei, P. A., Haghighat, F.: Approaches to study urban heat island–abilities and
631 limitations. Build. Environ. 45(10): 2192-2201, 2010.

632 Mitraka, Z., del Frate, F., Chrysoulakis, N., and Gastellu-Etchegorry, J. P.: Exploiting
633 earth observation data products for mapping local climate zones. Joint Urban Remote
634 Sensing Event (JURSE). 1-4, 2015.

635 Nakamura, I., and Llasat, M. C.: Policy and systems of flood risk management: a
636 comparative study between Japan and Spain. Nat. Hazards. 87(2): 919-943, 2017.

637 Nations, United.: World population prospects: The 2015 revision. United Nations Econ.
638 Soc. Aff. 33(2): 1-66, 2015.

639 Nayak, S. G., Shrestha, S., Kinney, P. L., Ross, Z., Sheridan, S. C., Pantea, C. I., Hsu, W.
640 H., Muscatiello, N., and Hwang, S. A.: Development of a heat vulnerability index for
641 New York State. Public health. 161: 127-137, 2018.

642 Oke, T. R.: The energetic basis of the urban heat island. Q. J. Roy. Meteor. Soc. 108(455):
643 1-24, 1982.

644 Pachauri, R. K., Allen, M. R., Barros, V. R., Broome, J., Cramer, W., Christ, R., Church
645 J. A., Clarke, L., Dahe, Q., Dasgupta, P., Dubash, N. K., Edenhofer, O., Elgizouli, I.,
646 Field, C. B., Forster, P., Friedlingstein, P., Fuglestvedt, J., Gomez-Echeverri, L.,
647 Hallegatte, S., Hegerl, G., Howden, M., Jiang, K., Jimenez Cisneroz, B., Kattsov, K., Lee,
648 H., Mach, K. J., Marotzke, J., Mastrandrea, M. D., Meyer, L., Minx, J., Mulugetta, Y.,
649 O'Brien, Oppenheimer, M., Pereira, J. J., Pichs-Madruga, R., Plattner, G. K., Pörtner, H.
650 O., Power, S. B., Preston, B., Ravindranath, N.H., Reisinger, A., Riahi, K., Rusticucci,
651 M., Scholes, R., Seyboth, K., Sokona, Y., Stavins, R., Stocker, T. F., Tschakert, P., van

652   Vuuren, D., and van Ypserle, J.P.: Climate change 2014: synthesis report. Contribution
653   of working groups I, II and III to the fifth assessment report of the intergovernmental
654   panel on climate change. R. Pachauri, L. Meyer (Eds.), IPCC, Geneva, Switzerland.
655   ISBN: 978-92-9169-143-2, 2014.

656   Rosenzweig, C., Solecki, W. D., Romero-Lankao, P., Mehrotra, S., Dhakal, S., and Ali
657   Ibrahim, S.: Climate change and cities. Second assessment report of the urban climate
658   change research network. New York: Cambridge University Press. Retrieved from:
659   http://www.cambridge.org/ws/academic/subjects/earth-and-environmental-
660   science/climatology-and-climate-change/climate-change-and-cities-second-assessment-
661   report-urban-climate-change-research-network, 2018.

662   Sheridan, S. C., and Dixon, P. G.: Spatiotemporal trends in human vulnerability and
663   adaptation to heat across the United States. Anthropocene. 20: 61-73, 2016.

664   Skarbit, N., Stewart, I. D., Unger, J., and Gál, T.: Employing an urban meteorological
665   network to monitor air temperature conditions in the 'local climate zones' of Szeged,
666   Hungary. Int. J. Climatol. 37: 582-596, 2017.

667   Skarbit, N., Gal, T., and Unger, J.: Airborne surface temperature differences of the
668   different Local Climate Zones in the urban area of a medium sized city. Joint Urban
669   Remote Sensing Event (JURSE). 1-4, 2015.

670   Smid, M., Russo, S., Costa, A. C., Granell, C., and Pebesma, E.: Ranking European
671   capitals by exposure to heat waves and cold waves. Urban Climate, 27, 388-402, 2019.

672   Sobrino, J. A., and Irakulis, I.: A Methodology for Comparing the Surface Urban Heat
673   Island in Selected Urban Agglomerations Around the World from Sentinel-3 SLSTR
674   Data. Remote Sensing, 12(12), 2052, 20202.

675   Stewart, I. D.: A systematic review and scientific critique of methodology in modern
676   urban heat island literature. Int. J. Climatol. 31(2): 200-217, 2011.

677   Stewart, I. D., and Oke, T. R.: Local climate zones for urban temperature studies. B. Am.
678   Meteorol. Soc. 93(12): 1879-1900, 2012.

679   Stewart, I. D., Oke, T. R., and Krayenhoff, E. S.: Evaluation of the 'local climate zone'
680   scheme using temperature observations and model simulations. Int. J. Climatol. 34(4):
681   1062-1080, 2014.

682   Tromeur, E., Ménard, R., Bailly, J. B., and Soulié, C.: Urban vulnerability and
683   resilience within the context of climate change. Nat. Hazards Earth Syst. Sci., 12(5),
684   2012.

685   Unger, J., Skarbit, N. and Gál, T.: Evaluation of outdoor human thermal sensation of local
686   climate zones based on long-term database. International Journal of Biometeorology,
687   62(2), 183–193, 2018.

688   UNISDR, UNOFDRR.: Terminology on disaster risk reduction. Geneva, Switzerland,
689   2009.

690   Verdonck, M. L., Demuzere, M., Hooyberghs, H., Beck, C., Cyrys, J., Schneider, A.,
691   Dewulf, R., and Van Coillie, F.: The potential of local climate zones maps as a heat stress
692   assessment tool, supported by simulated air temperature data. Landscape Urban plan.
693   178: 183-197, 2018.

694   Voogt, J. A., and Oke, T. R.: Thermal remote sensing of urban climates Remote Sens.
695   Environ. 86(3): 370-384, 2003.

696   Wang, R., Ren, C., Xu, Y., Lau, K. K. L., and Shi, Y.: Mapping the local climate zones
697   of urban areas by GIS-based and WUDAPT methods: A case study of Hong Kong. Urban
698   Clim. 24: 567- 576, 2017.

699   Weber, S., Sadoff, N., Zell, E., and de Sherbinin A.: Policy-relevant indicators for
700   mapping the vulnerability of urban populations to extreme heat events: A case study of
701   Philadelphia. Appl. Geogr. 63: 231-243, 201.5, 2015.

702   Wolf, T., and McGregor G.: The development of a heat wave vulnerability index for
703   London, United Kingdom. Weather and Climate Extremes. 1: 59-68, 2013

704   Xu, Z., Sheffield, P. E., Hu, W., Su, H., Yu, W., Qi, X., and Tong S.: Climate change and
705   children's health- A call for research on what works to protect children. I Int. J. Environ.
706   Res. Public Health. 9(9): 3298-3316, 2012.

707

708   a   b
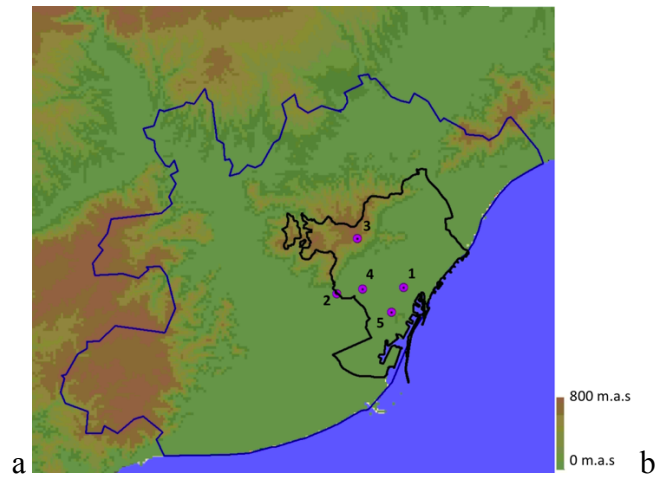
709 **Figure 1. a) Location of the Metropolitan Area of Barcelona (AMB), b) Domain used to run the**
710 **UrbClim model. The blue line marks the border of the AMB, while the black line shows the**
711 **municipality of Barcelona. The numbers indicate the weather stations used to assess the LCZ-T**
712 **relationship.**

713

714
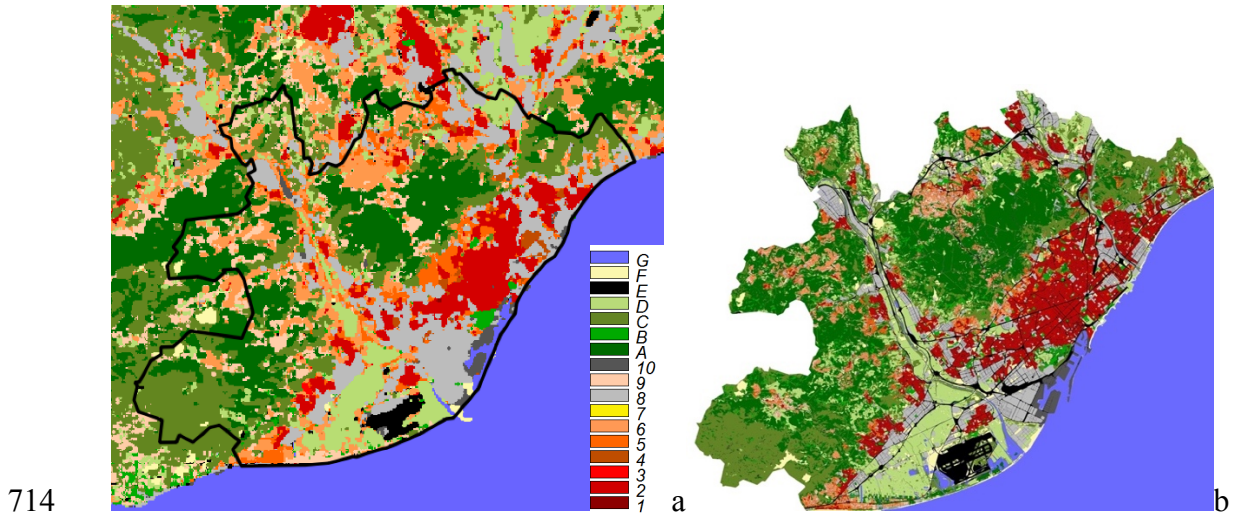
715   **Figure 2. LCZ maps: a) WUDAPT method, b) LCLU method.**

716

717
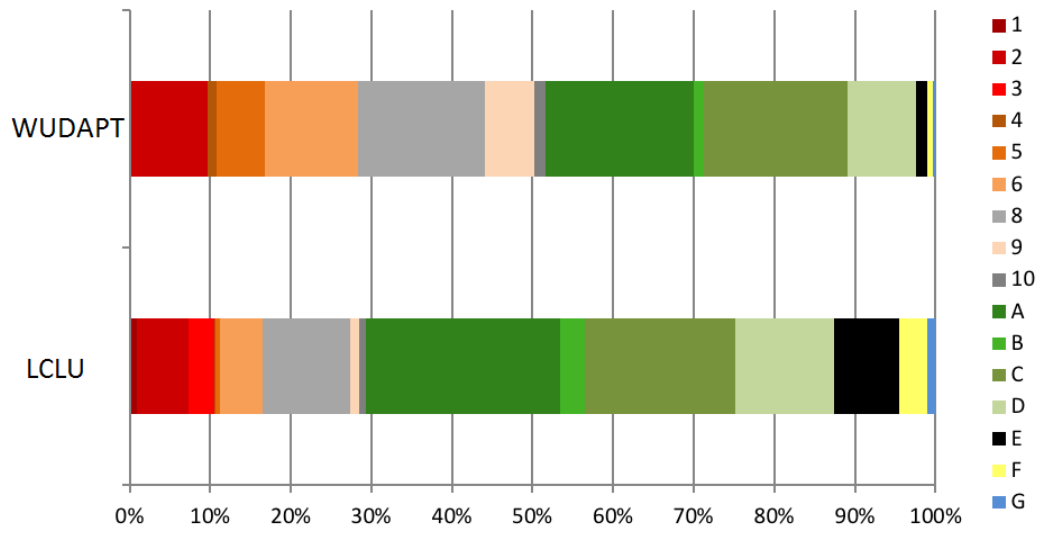
Figure 3. Percentage of the area covered by each LCZ using WUDAPT and LCLU inside AMB.

719

720

721
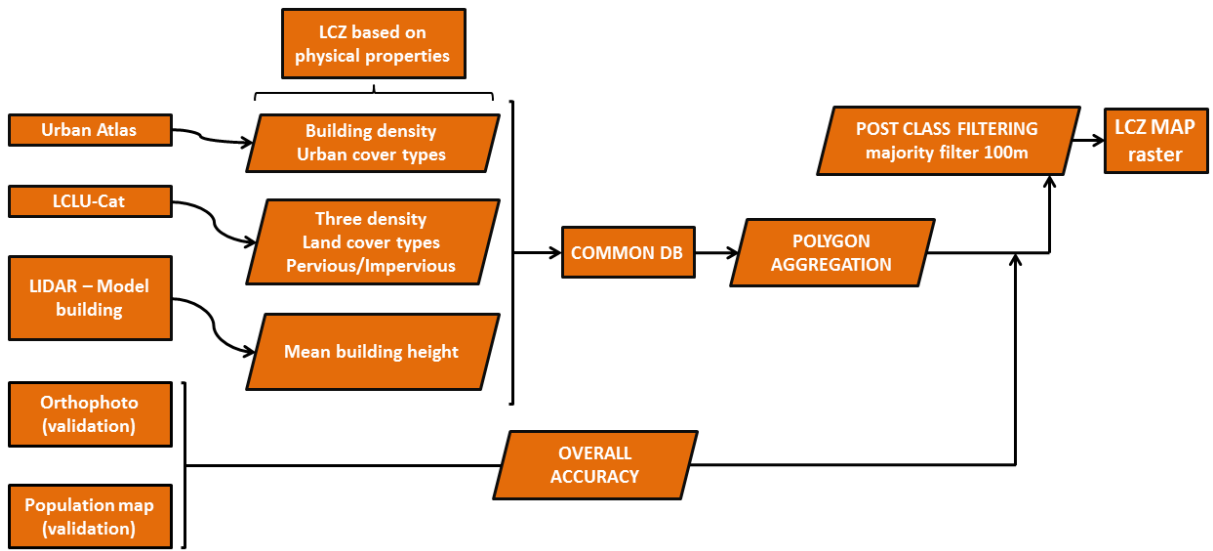
722

723   **Figure 4. Workflow used to obtain the LCZ LCLU model.**

724
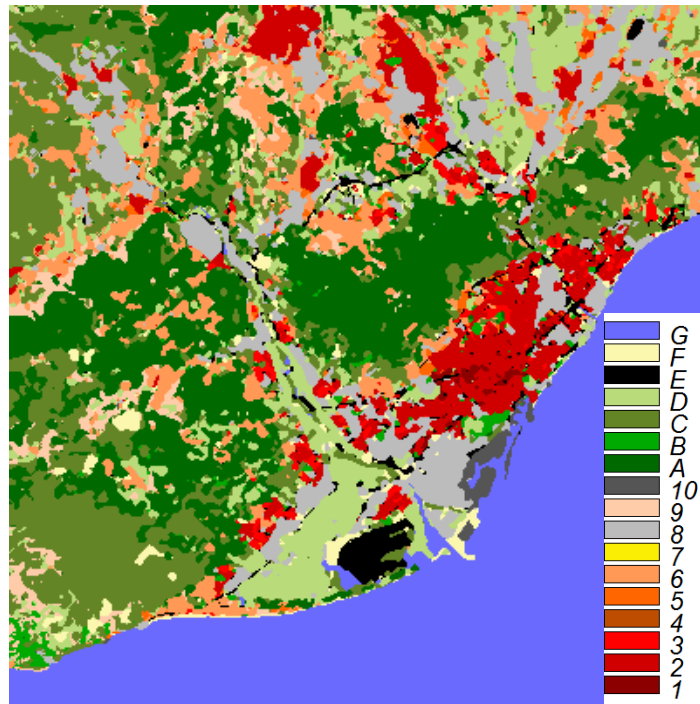
725

726   **Figure 5. LCZ used in the UrbClim model based on workflow showed in Fig. 4.**

727

728
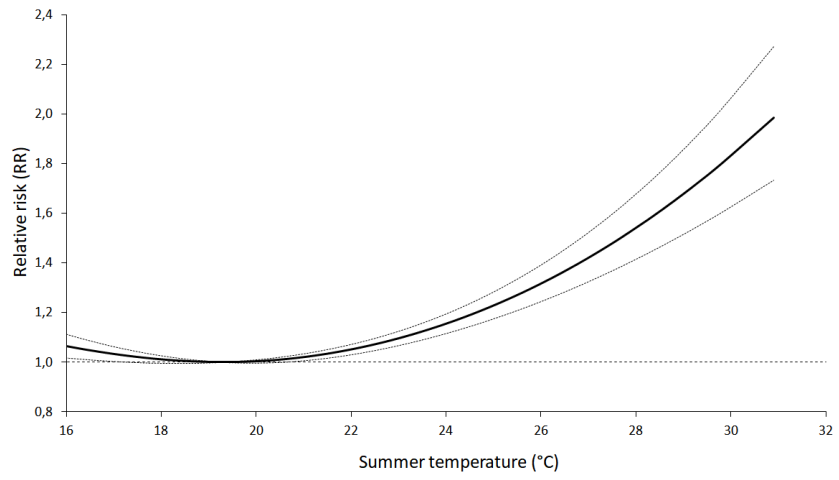
Figure 6. Relative risk (RR) curve based on mortality due to summer daily temperature (JJA) in Barcelona for the 1980 - 2015 period (Achebak et al., 2018).

729
730

731

732

733
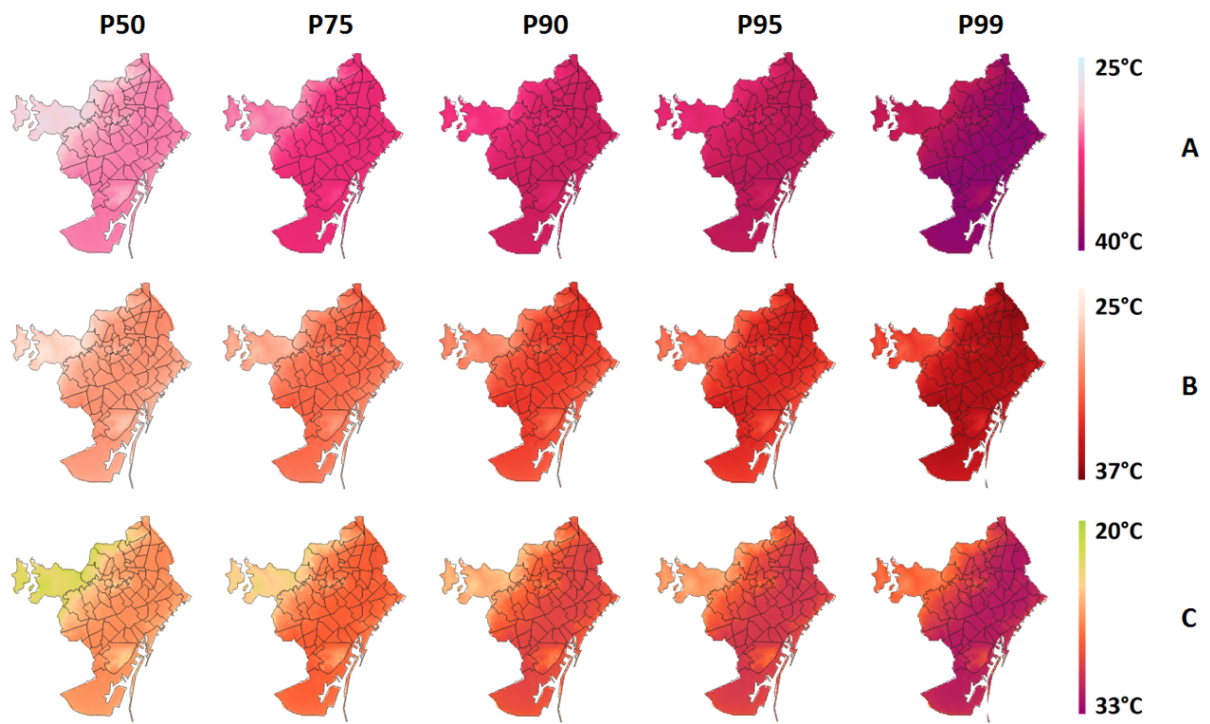
Figure 7. Climatological conditions in summer modelled by UrbClim (1987 - 2016): A) HUMIDEX, B) Daily maximum temperature, C) Daily mean temperature, for the different distributions (P 50, P 75, P 90, P 95 and P 99).

738
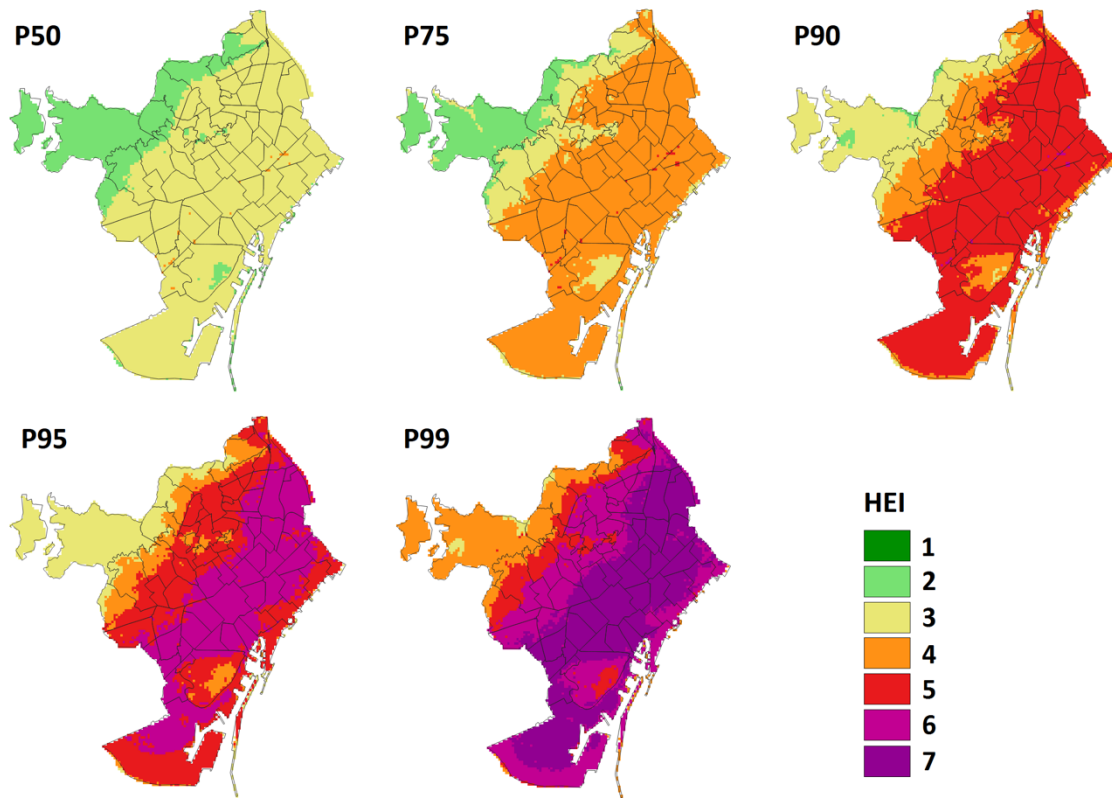
Figure 8. Maps of HEI for the different probability distributions proposed (P 50, P 75, P 90, P 95 and P 99).

739
740

741
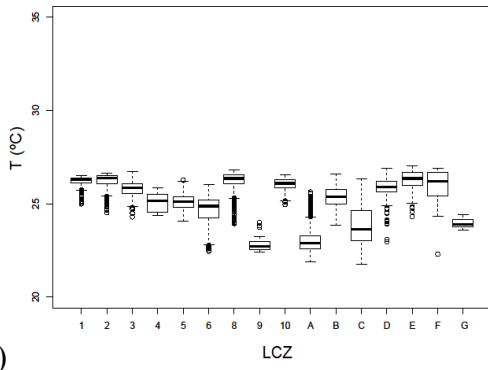
742   a)
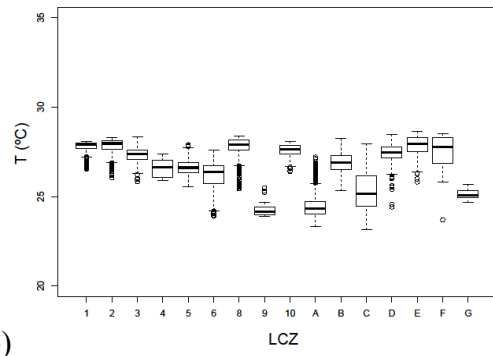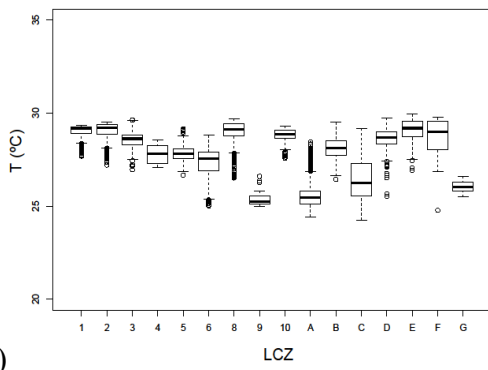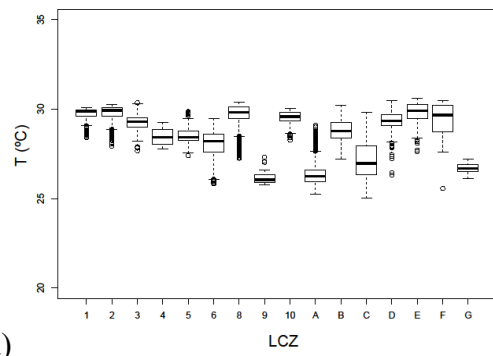
743   c)   d)
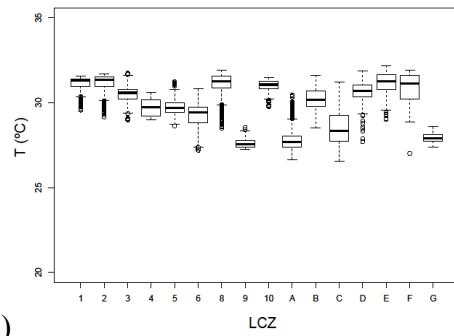
744   e)

745   **Figure 9. Box plots for the thermal characterisation of the LCZ for different distributions: a) P 50,**

746   **b) P 75, c) P 90, d) P 95 and e) P 99. (See S1 for LCZ features)**
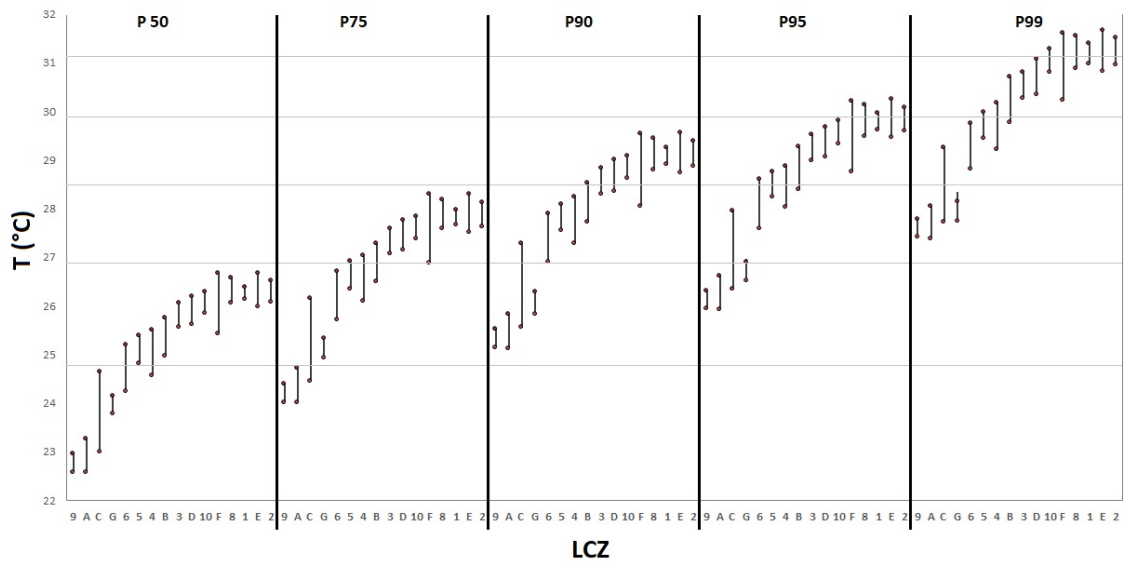
747

748   **Figure 10. Characterisation of every LCZ with the daily mean temperature (1987 - 2016) for each**
749   **probability scenario. Each bar shows P 25 and P 75, around the median for each LCZ (ordered**
750   **from lowest to highest temperature). The grey horizontal lines are the different HEI scenarios (2 to**
751   **7, lower to high).**

752

753
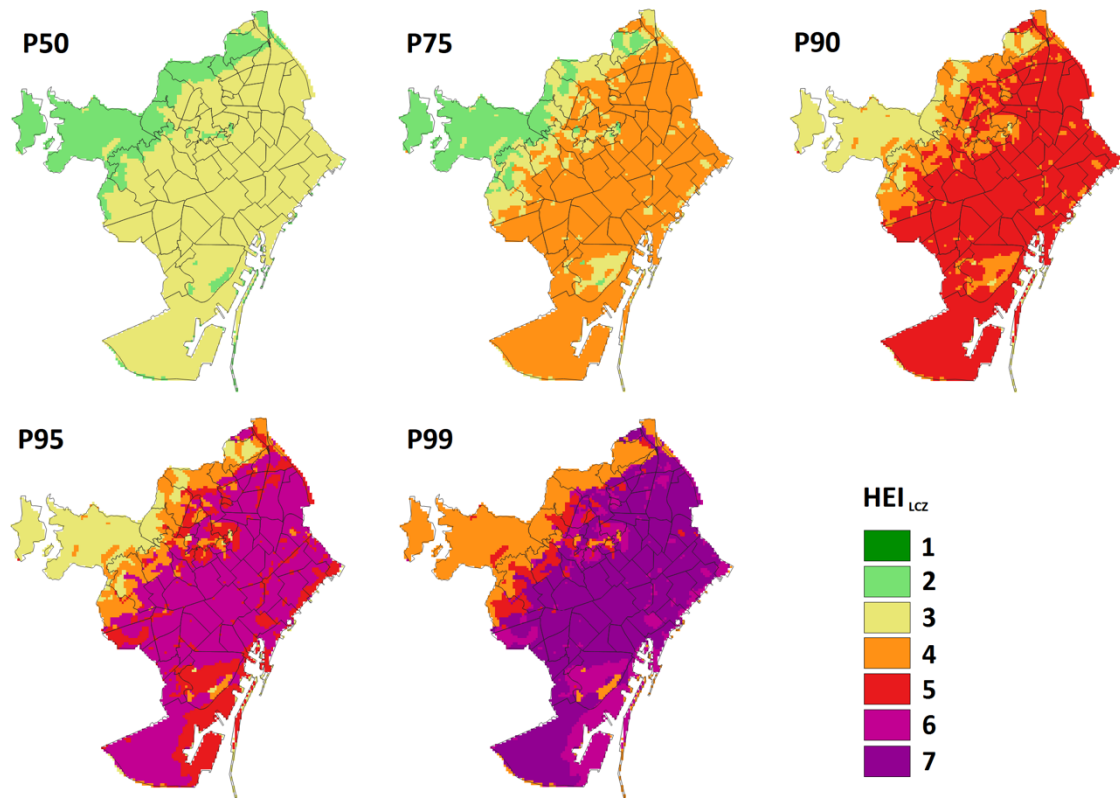
Figure 11. Cartography of the heat exposure (HEI) in basis to thermal characterization of Barcelona by LCZs for different percentiles (LCZ - T) as shown in Table 3.

756

757

Layer	Information	Spatial Resolution	Year	Format
Urban Atlas	20 categories of urban fabric	5 m	2010	Vector cartography
LCLU-Cat	241 categories	0.25 m	2010	Vector cartography
Building Heights	Height (m) (LIDAR)	0.5 m	2014	Vector cartography
Orthophoto	Mosaic of aerial photos	0.25 m	2016	Raster cartography
Population	Population by ages	62.5, 125, 250 m	2016	Vector cartography
LANDSAT 8	05/03/2015	30m	2015	Raster satellite

758   **Table 1. Vector and raster cartographic data and satellite images used to map the LCZ - LCLU and**
759   **LCZ - WUDAPT methods.**

760

761

762

ID	Weather Stations	Series	Years	LCZ	Z (m.a.s)	Variable
1	Raval	1997-2016	19	2	33	T daily
2	Zona Universitària	1997-2016	19	C	79	T daily
3	Fabra	1987-2016	29	A	411	T daily
4	Can Bruixa	1987-2015	28	2	61	T daily
5	Montjuïc	2004-2015	11	B	90	T daily

763 **Table 2. Weather stations in Barcelona used to assess the LCZ - T relationship based on daily mean**
764 **temperatures.**

765

766

RR	HEI	ºC
1.0	1	18 -20
1.2	2	20 -24.7
1.4	3	24.7 -26.9
1.6	4	26.9 -28.5
1.8	5	28.5 -29.8
2.0	6	29.8 -31.1
>2.0	7	>31.1

767

768

769

770

771

772 **Table 3. Temperature thresholds associated to heat exposure caused by high temperatures in basis**
773 **to figure 5. Heat Exposure Index (HEI) is assigned to each temperature range.**

774

LCZ	P 50	P 75	P 90	P 95	P 99
1	0.301	0.325	0.349	0.363	0.419
2	0.356	0.379	0.396	0.401	0.475
3	0.450	0.468	0.486	0.489	0.552
4	0.528	0.530	0.535	0.522	0.569
5	0.467	0.488	0.504	0.500	0.541
6	0.821	0.841	0.872	0.843	0.804
8	0.465	0.499	0.527	0.531	0.580
9	0.456	0.474	0.461	0.441	0.379
10	0.319	0.338	0.339	0.338	0.322
A	0.686	0.712	0.725	0.705	0.649
B	0.554	0.580	0.603	0.616	0.641
C	1.090	1.128	1.168	1.128	1.088
D	0.550	0.572	0.596	0.586	0.612
E	0.530	0.561	0.599	0.595	0.678
F	0.848	0.918	0.960	0.955	0.978
G	0.224	0.265	0.297	0.294	0.289

775 **Table 4. Standard deviations for the LCZs for the different percentiles of temperature.**

776

777

	DIST	OB	UC	LCZ-T	ΔOB−UC	ΔOB−LCZ-T
1-Raval (LCZ 2)	P50	25.6	26.1	26.1	0.5	0.5
	P75	26.8	27.6	27.6	0.8	0.8
	P90	27.8	28.9	28.9	1.1	1.1
	P95	28.5	29.6	29.6	1.1	1.1
	P99	30.2	31.1	30.9	0.9	0.7
2-ZU (LCZ C)	P50	24.5	24.7	24.6	0.2	0.1
	P75	25.8	26.2	26.2	0.4	0.4
	P90	26.6	27.3	27.3	0.7	0.7
	P95	27.2	28.1	27.9	0.9	0.7
	P99	28.5	29.5	29.2	1	0.7
3-Fabra (LCZ A)	P50	23.1	23.1	22.9	0	-0.2
	P75	24.6	24.7	24.3	0.1	-0.3
	P90	25.9	25.8	25.5	-0.1	-0.4
	P95	26.5	26.6	26.2	0.1	-0.3
	P99	27.3	27.5	27.7	0.2	0.4
4-C. Brüixa (LCZ B)	P50	25.2	26.1	25.4	0.9	0.2
	P75	26.8	27.6	26.9	0.8	0.1
	P90	27.9	28.9	28.1	1	0.2
	P95	28.6	29.6	28.8	1	0.2
	P99	30	30.9	30.2	0.9	0.2
5-Montjuïc (LCZ B)	P50	24.8	25.2	25.0	0.4	0.2
	P75	26.3	26.8	26.5	0.5	0.2
	P90	27.3	28	27.7	0.7	0.4
	P95	27.8	28.6	28.4	0.8	0.6
	P99	29.1	30.1	29.8	1	0.7

778   **Table 5. Temperature for each distribution/scenario (DIST) and weather station observed (OB),**
779   **modelled by UrbClim (UC) and estimated from the distribution of temperature (the mean value is**
780   **taken) for each LCZ (LCZ-T). The difference (Δ) between them is also showed. All the values are**
781   **expressed in º C.**

782

MODEL	P50	P75	P90	P95	P99
Underestimate	284	671	1711	2789	2289
Good	9687	8762	8175	6316	6823
Overestimate	247	785	332	1103	1106
% correct	95	86	80	62	67
RMSE	0.23	0.38	0.45	0.62	0.58

783 **Table 6. Number of pixels where the HEI obtained through the LCZ-T model (Figure 11)**

784 **underestimate, overestimate or coincide with the HEI provided by the Urban Climate Model**

785 **(Figure 6) for the different scenarios. Percentage of coincidences and RMSE are also showed.**

786

787